Automatic Tuning of Augmented PIDs for Active Magnetic Bearings Supporting Turbomachinery

Automatic Tuning of Augmented PIDs for Active Magnetic Bearings Supporting Turbomachinery

Giovanni Donati, Michele Basso, Marco Mugnaini, *Senior Member, IEEE*, and Massimiliano Ortiz Neri

***Abstract*—In industry, augmented proportional–integral–derivative controllers are still frequently employed with active magnetic bearings supporting turbomachinery. Despite their simple single-input-single-output (SISO) structure, the process of tuning such controllers remains iterative and manual, demanding considerable time from experienced engineers to ensure the rotodynamic system meets performance requirements. This article introduces an innovative method that facilitates engineers in incorporating design requirements by translating performance criteria into mathematical constraints and objectives. These are then exploited by an advanced nonsmooth optimization algorithm to automatically adjust controller parameters, accounting for system uncertainties and varying operating conditions. The proposed procedure offers a flexible and innovative approach for automatically designing robust SISO-based controllers for turbomachinery equipped with active magnetic bearings. This significantly reduces the time required for manual tuning by experienced engineers while ensuring all performance objectives are met. An implementation of this tuning method on a real turbomachine is presented, and the results are discussed with a particular focus for the application in the oil and gas field.**

***Index Terms*—Active magnetic bearings (AMBs), augmented proportional—integral–derivative (PID), automatic tuning, rotodynamic system.**

I. Introduction

ACTIVE magnetic bearings (AMBs) are increasingly being utilized in various rotodynamic applications, ranging from small medical turbo molecular pumps to large oil and gas compressors in the Megawatt range. AMBs offer a significant advantage over traditional bearings because they eliminate friction between the stator and rotor, resulting in numerous benefits for the system. This absence of friction allows for higher rotation speeds, increases system efficiency, eliminates the need for cumbersome lubrication systems that are necessary for conventional oil film bearings, and, by reducing wear, the need for frequent preventive maintenance, as highlighted e.g., in Schweitzer's [1] work. In addition, AMBs are active systems that can change their dynamic behavior, allowing for remote control and real-time adjustments of their characteristics, and vibration control. However, AMB systems are complex mechatronic systems composed of different elements, including controllers, position sensors, and actuators and, because of the actuators power limitations, AMBs have a lower load capacity than classic bearings. Moreover, AMB are intrinsically unstable systems that require stabilizing feedback controls based on rotor position measurements therefore, the controller design becomes a crucial aspect. The design of the controller and the choice of the other elements determine the bearing dynamic behavior that is the resulting bearing damping and stiffness. Various controller structures and design processes have been applied in the literature, the most used controller structures are summarized in [2] and [3]. These include flux density controllers [4], gain-scheduling H-infinite [5], [6], sliding mode control [7], μ-synthesis [8], fuzzy logic [9] and, recently, artificial neural networks [10]. Each structure requires a different design process that considers the specific characteristics of the turbomachine and the desired goals. Although these techniques produce controllers with excellent performance, they often result in overly complex controllers, which are not commonly adopted in industry. Despite the availability of numerous alternatives, augmented proportional–integral–derivative (PID) controllers remain the most widely used controller structures in industrial AMB applications due to their simplicity. In particular, augmented PIDs are a popular choice in industry due to their versatility, accuracy, efficiency, and cost-effectiveness. Above all, the fixed structure (and order) of PID controllers is the primary reason for their widespread adoption in industry, as it ensures compatibility with existing hardware implementations.

Moreover, they can be easily adjusted to accommodate changes in the process, making them robust to evolving applications, such as a turbomachinery process in which the system may change its dynamics over time (e.g., caused by process gas on rotor components).

Despite their simple structure, the tuning phase for these controllers is a critical process that frequently necessitates numerous manual iterative steps relying on rules derived from experience.

Manuscript received 7 February 2024; revised 5 April 2024; accepted 27 May 2024. Recommended by Technical Editor Z. Bi and Senior Editor Y.-J. Pan. This work was supported by Baker Hughes Company. *(Corresponding author: Giovanni Donati.)*

Giovanni Donati and Michele Basso are with the Department of Information Engineering, University of Florence, 50121 Florence, Italy (e-mail: giovanni.donati@unifi.it; michele.basso@unifi.it).

Marco Mugnaini is with the Department of Information Engineering and Mathematics, University of Siena, 53100 Siena, Italy (e-mail: marco.mugnaini@unisi.it).

Massimiliano Ortiz Neri is with Baker Hughes Company, 50127 Florence, Italy (e-mail: massimiliano.ortizneri@bakerhughes.com).

Color versions of one or more figures in this article are available at https://doi.org/10.1109/TMECH.2024.3407674.

Digital Object Identifier 10.1109/TMECH.2024.3407674

For example, [11], [12], and [13] described some standard tuning procedures for this type of controllers. The tuning procedure presents a significant challenge, not only because of the complex nature of the inherently unstable AMB systems but also due to the need of complying with the strict regulations governing turbomachinery supported by AMBs [14], particularly in the oil and gas industry [15].

In order to address these challenges, in this work the authors propose an innovative model-based method for automatically tuning augmented PID controllers, offering a new approach to both optimize the system performance, comply with the regulations and accounting for the physical limitations of the real system. The proposed approach relies on the application of a nonsmooth optimization technique [16], [17], [18] and exploits a simple and novel procedure for incorporating regulation requirements and "best practice" rules in the optimization process, providing the mathematical translation of the rules commonly used in the AMB oil and gas field. Aiming for the same objectives as manual tuning, the primary difference lies in the efficiency of achieving these results: whereas manual tuning requires substantial time and effort from experienced engineers to systematically explore various parameter combinations, the automatic technique updates this process through optimization algorithms. Furthermore, a pre-specified set of uncertain parameters is employed to compute a robust controller capable of handling the uncertainties associated with the rotor model and, importantly, addressing the effects of rotational speed on the model. Since the automatic tuning method is based on the system model, one of the fundamental aspects is to ensure that the modeled system well represents the real one. This aspect can be successfully addressed by different techniques [19], [20]. In this article, fine tuning of finite element (FE) model based on rotor frequency responses measurements [20] was used which allows for successfully applying model-based control synthesis methods. By applying nonsmooth optimization, a system local minimum linked to the specified requirements and constraints that the system must comply with is found and the augmented PIDs parameters are automatically chosen. Moreover, the proposed approach enables the fine-tuning of parameters of a previously tuned controller when the system condition changes, for example in case of soft faults, as studied for example in [21].

The authors' automatic tuning method is a better alternative to the multiobjective genetic algorithms (MOGAs) applied to the same problem, as for example in [22]. The first issue with MOGA lies in the difficulty of translating the various system requirements into a mathematical form that MOGA can effectively handle. Furthermore, unlike the proposed tuning method, the results obtained from MOGAs are adversely affected by system complexity, and they struggle to handle variable operation conditions, like for example variable rotational speed, and system uncertainties.

This article focuses in particular on AMB systems operating in the oil and gas field since they are particularly challenging due to the system complexity and to the strict regulations in force for this type of system.

The rest of this article is organized as follows. In Section II, the AMB system modeling is introduced, with a particular focus on the AMB theoretical background. Section III formulates the problem and describes the proposed tuning method. The proposed method was applied to a real expander–compressor whose structure is described in Section IV, which also presents the system performance goals and constraints used. In Section V the experimental results are presented and discussed. Finally, Section VI concludes this article.

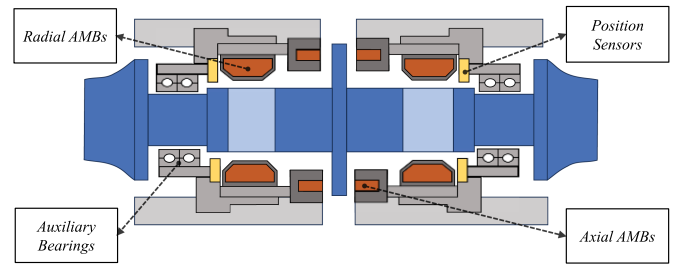

Fig. 1. Schematic of an AMB system plant.

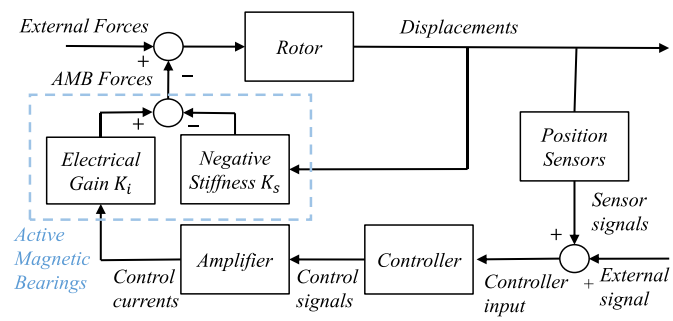

Fig. 2. AMB system block diagram.

II. System Description and Dynamic Modeling

A. AMB System Modeling

Fig. 1 shows a typical turbomachine supported by AMBs. AMBs are formed by electromagnets to make the rotor levitate centered in the air gap relative to the stator. For simplicity, this study focuses only on radial AMBs, each composed of four identical electromagnets and two orthogonal control axes, since the rotor axial symmetry. By adjusting the current in these electromagnets, different forces on the rotor can be generated. The force, F_z, generated along control axis Z depends on current and displacement. For small deviations from the nominal working point, a linear relationship can be expressed [23]

$$F_z = k_i\, i_z - k_s z \tag{1}$$

where z is the rotor displacement along the control axis Z with respect to the nominal conditions, k_i and k_s are the so-called electrical gain and negative stiffness, respectively, which depend on the geometrical parameters of the bearings and on the nominal operating conditions. Due to the negative stiffness k_s, AMBs are always inserted in a stabilizing closed loop, summarized in Fig. 2. The AMB closed-loop system is composed of position sensors, that monitor the rotor position, a controller, that determines the control signals from the position sensor outputs, the amplifiers, that convert the control signals into currents driving the AMBs and, of course, the electromagnets (actuators), that

form the AMBs. To model the closed-loop system dynamics, a state–space formulation of every component was used. In particular, the rotor radial state–space model was found by using a finite element method using a Timoshenko modeling; a detail description of the modeling formulation used can be found in [24] or [25]. Therefore, the rotor dynamics can be described by the following differential equation:

$$M\ddot{q} + (C + \Omega C_g)\,\dot{q} + (K - K_s)\,q = F_{\text{AMB}} + F_{\text{ext}} \tag{2}$$

where M is the mass matrix, C is the damping matrix (normally due only to the damping of the material of the rotor), C_g is the gyroscopic matrix, K is the stiffness matrix, Ω is the rotor rotational speed, F_{ext} are the external forces acting on the rotor, F_{AMB} is the AMB control force depending on the control currents, q is the vector that represents the position and rotation of every node of the rotor, and K_s is the matrix of negative stiffnesses. Because of the Ω term in (2), the rotor model is linear time invariant only for a fixed rotor speed.

From (2), the rotor state–space model can be written

$$\begin{aligned} \dot{X}_R &= A_R\,X_R + B_R\,(F_{\text{AMB}} + F_{\text{ext}}) \\ q &= C_R\,X_R \end{aligned} \tag{3}$$

where

$$X_R = \begin{bmatrix} q \\ \dot{q} \end{bmatrix},\ A_R = \begin{bmatrix} [0] & I \\ -M^{-1}\,(K - K_s) & -M^{-1}\,(C + \Omega C_g) \end{bmatrix}$$

$$\mathrm{B_R} = \begin{bmatrix} [0] \\ M^{-1} \end{bmatrix},\ C_R = \begin{bmatrix} I & [0] \end{bmatrix}.$$

Due to the decentralized nature of the system, diagonal linear models are also used to describe the dynamics of the AMB electrical components, taking into consideration their individual characteristics and specifications. So, the sensors transfer function, $G_s(s)$, the actuators transfer function, $G_{\text{act}}(s)$, and the controller transfer function, $G_c(s)$, were found. Finally, the transfer function $G_B\,(s) = G_{\text{act}}\,(s)G_c(s)G_s(s)$ can be defined. Using a canonical form, $G_B(s)$ can be easily described by the following state–space system:

$$\begin{aligned} \dot{X}_B &= A_B\,X_B + B_B q \\ F_{\text{AMB}} &= C_B\,X_B \end{aligned} \tag{4}$$

where X_B is the state and (A_B, B_B, C_B) are the matrices of the second state–space model. To obtain a state space–space model of the whole closed-loop system, combining (3) with (4) the following equation can be written:

$$\begin{aligned} \frac{d}{dt}\begin{bmatrix} X_R \\ X_B \end{bmatrix} &= \begin{bmatrix} A_R & B_R C_B \\ B_B C_R & A_B \end{bmatrix}\begin{bmatrix} X_R \\ X_B \end{bmatrix} + \begin{bmatrix} B_R \\ [0] \end{bmatrix} F_{\text{ext}} \\ &= A\begin{bmatrix} X_R \\ X_B \end{bmatrix} + BF_{\text{ext}}. \end{aligned} \tag{5}$$

The above-mentioned allows for studying the AMB performance and to evaluate the compliance with the AMB regulations of the closed-loop system that is obtained by tuning the controller.

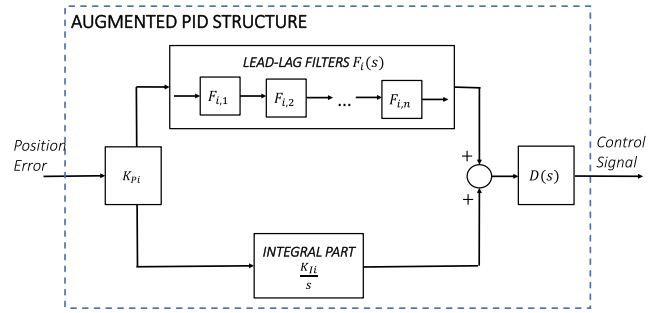

Fig. 3. This scheme describes a generic augmented PID structure [11].

B. Augmented PID Structure

As mentioned earlier, this article uses a fixed structure for the controller, specifically an augmented PID with a decentralized design, i.e., $G_c\,(s) = \text{diag}(G_{c1}(s), \ldots, G_{cN}(s))$ where N is the number of control axes. Although the rotor system is inherently a multiple input multiple output (MIMO) system, each control axis is independently managed by a SISO augmented PID. A generic augmented PID is composed of a series of elements that act as a proportional part, an integral part, and a derivative part. The following equation describes the transfer function, $G_{ci}(s)$, of the ith generic single augmented PID in the Laplace domain:

$$G_{ci}\,(s) = K_{Ci}\left(\frac{K_{Ii}}{s} + F_i\,(s)\right)D\,(s) \tag{6}$$

where K_{Ci} and K_{Ii} are constants, $F_i(s)$ represents the dynamics of a number of lead-lag filters that are used implement a derivative action in specific frequency bands whereas $D(s)$ describes the effect of the digital to analog converter (DAC) accounting also for the delay due to the sampling time. Fig. 3 summarizes the structure of a generic augmented PID. The implemented augmented PID structure in AMB industrial applications offers several distinct advantages, as elucidated by Defoy et al. [12]. This configuration features a parallel arrangement of the integral component, as in classical PIDs. Consequently, the impact of the integral action is confined to low frequencies where rotor vibrational modes are absent. As its primary objective is to maintain the rotor central position within the air gap, the integral action remains negligible at high frequencies, not contributing to destabilize the system. However, its significance becomes pronounced at lower frequencies, aligning with the inherently slow dynamics of turbomachine changes. $F_i(s)$ is the cascade product of different filters that can be of the first or of the second order type. The structure of the jth filter composing $F_i(s)$, respectively of the first and second order and used also for example in [12], can be described as follows:

$$F_{i,j}\,(s) = \frac{\tau_{i,j}S + 1}{\alpha_{i,j}\tau_{i,j}S + 1} \tag{7}$$

$$F_{i,j}\,(s) = \frac{\frac{s^2}{\omega_{zi,j}^2} + \frac{2\delta_{zi,j}}{\omega_{zi,j}}S + 1}{\frac{s^2}{\omega_{pi,j}^2} + \frac{2\delta_{pi,j}}{\omega_{pi,j}}S + 1} \tag{8}$$

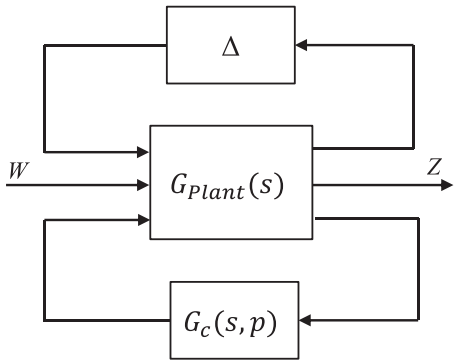

Fig. 4. LFT plant with real parametric uncertainties and tunable parameters.

where $\tau_{i,j} > 0,\ \alpha_i > 0$ are the tunable parameters of the first order filters and $0 < \delta_{zi,j}\langle 1,\ \omega_{zi,j}\rangle 0,\ 0 < \delta_{pi,j}\langle 1,\ \omega_{pi,j}\rangle 0$ are the tunable parameters of the second order filters. These tunable parameters have upper and lower bounds linked to the realizability of the real control system. By tuning the parameters, the derivative action can be obtained only in the frequency ranges in which the filters provide a phase lead. In detail, the first order filters have a quite distributed action in the frequency domain and are used to stabilize the rotor rigid modes, in contrast the second order filters are more versatile and can be used in many different ways, for example as notch filters to drop the system gain in a narrow frequency range, e.g., containing rotor modes. The tuning goal is to find the controller parameters, which satisfy the system constraints and optimize the system performance.

III. Augmented PID Automatic Tuning

The goal of AMB controller tuning is to define the controller parameters ensuring that the closed loop system satisfies the requirements and desired performance. The multitude of requirements, along with their diverse nature, combined with plant uncertainties, presents a significant obstacle to controller tuning. The proposed automatic tuning procedure employs a nonsmooth optimization methodology developed by Apkarian et al. [16], [17], [18], effective for fixed-structure controller tuning against various requirements and in the presence of parametric uncertainties [26]. To exploit this procedure, the studied system is described by a linear fractional transformation (LFT) plant [27], with the schematization shown in Fig. 4, in which the parametric uncertainties Δ (considered real) are explicated, $G_c(s,p)$ is the transfer function of the controller with n tunable parameters $p \in \mathbb{R}^n$ and $G_{\text{Plant}}(s)$ is the open loop plant system transfer function, in a reference condition, i.e., with all the uncertainties null. The uncertainty matrix Δ is assumed diagonal $\Delta = \text{diag}[\delta_1 \text{Ir}_1, \ldots, \delta_\text{m} \text{Ir}_\text{m}]$ with δ_i representing real parametric system uncertainties, and Ir_i giving the number of repetitions of δ_i. This system rearranging is easily obtainable since the functions $G_c(s,p), G_s(s)$, and $G_{\text{act}}(s)$ are diagonal and the uncertainty diagonal matrix Δ can be easily found as demonstrated in [28]. Therefore, the multiple requirements are divided into *soft* objectives (nice-to-have) and *hard* constraints (must-have). This leads to an optimization problem of the form

$$\begin{aligned} &\text{minimize}_{\delta\in\Delta} \max_{i=1,\ \ldots,n_o} \{\|T_{w_i\to z_i}\left(G_c\left(s,p\right),\delta\right)\|\} \\ &\text{subject to } \|T_{w_j\to z_j}\left(G_c\left(s,p\right),\delta\right)\| \le c,\ j=1,\ldots,n_c \end{aligned} \tag{9}$$

for every $\delta \in \Delta$, $c \in \mathbb{R}^+$ and $T_{w_i\to z_i}$ is used to represent the closed-loop map from signal w_i (ith component of the vector W in Fig. 4) to signal z_i(ith component of the vector Z in Fig. 4). The symbol $\|.\|$ refers to either the H_∞ or to the H_2 norms normally restricted to prescribed frequency ranges since the most of requirements, both in the frequency and time domains, can be easily translated in H norms requirements, as shown in [29].

Due to the inherent conservatism, outer methods, where the problem is relaxed on a convenient larger set $\tilde{\Delta} \supset \Delta$ and if solved it provides performance and robustness certificates, as for example the classic DK-iteration function [30], are computationally not convenient for large systems as the one considered in this work. Therefore, the implemented algorithm exploits a dynamic inner approximation that ensures a good tradeoff between performance and computational load, for which a relatively small set $\Delta_a \subset \Delta$ is considered and automatically and iteratively updated by applying a search procedure locating problematic parameter scenarios in Δ.

At first, the tunable parameters and the fixed blocks are separated, [31], to find the Standard Form which is equal to the one used in the classic H_∞ synthesis [32].

The requirements reported in (9) are aggregated and can be rewritten as

$$\begin{aligned} &\text{minimize } f\left(p,\delta\right) \\ &\text{subject to } g\left(p,\delta\right) \le 1 \end{aligned} \tag{10}$$

with

$$f\left(p,\delta\right) := \max_{i=1,\ldots,n_f} f_i\left(p,\delta\right),\ \ g\left(p,\delta\right) := \max_{i=1,\ldots,n_g} g_i\left(p,\delta\right)$$

where $\delta \in \Delta_a$, $f_i(p,\delta)$ and $g_i(p,\delta)$, describe each requirement, respectively *soft* and *hard*, of different nature and they are respectively scaled using each requirement minimum target value. Equation (10) reduces the computational cost by solving only the constraints that are nearly active, i.e., the constraints that can give a significant contribution. In fact, n_g and n_f represent, respectively, the number of the *hard* and *soft* requirements accounted for. Given the nonlinear, nonconvex, and nonsmooth nature of problem (10), a dedicated nonsmooth algorithm is employed for its solution. This algorithm is designed to minimize the worst-case value of the *soft* requirements while simultaneously enforcing the *hard* ones for every $\delta_i \in \Delta$. More specifically, the uncertainty set is initialized with a null set and the problem (10) is iteratively solved as described in the following. The constrained minimization is tackled defining the following objective function:

$$G_{p\eta}:\ \text{minimize } \Phi_\eta\left(p,\delta\right) := \max\left\{f\left(p,\delta\right),\ \eta g\left(p,\delta\right)\right\} \tag{11}$$

where η is a parameter adjusted by a Lagrangian method and that solve locally the Karush–Kuhn–Tucker condition [33] for criticality of program (10). Specifically, through a bisection

scheme η is corrected based on the constrain $g(p,\delta)$, i.e., η is increased when the constraint $g(p,\delta)$ is violated and vice versa. In other words, the problem (10) is solved through the solutions of a sequence of subproblems $G_{p\eta}$ where η is adjusted by a bisection scheme. By minimizing $\Phi_\eta(p,\delta)$, for the sequence of values of η that saturate the constraint $g(p,\delta) \leq 1$, solutions p^* are computed.

Since the considered control requirements $f_i(p,\delta)$ and $g_i(p,\delta)$ result as Lipschitz and even Clarke regular [34], the subproblem of minimizing Φ_η for a given η is tackled with an unconstrained algorithm, which is guaranteed to converge to local solutions for any even remote starting points [35], for which Clarke's subdifferentials $\partial G_{p\eta}(p,\delta)$ are computed using a convex hull rule

$$\partial G_{p\eta}(p,\delta) = \begin{cases} \partial f(p,\delta) & \text{if } f(p,\delta) > \eta g(p,\delta) \\ \eta \partial g(p,\delta) & \text{if } \eta g(p,\delta) > f(p,\delta) \\ \{\alpha \partial f(p,\delta) + (1-\alpha)\eta g(p,\delta) : \alpha \in [0,1] & \\ \qquad \text{if } \partial f(p,\delta) = \partial g(p,\delta). & \end{cases} \tag{12}$$

The results are critical points associated with local minima, compliant with the *hard* constraints. The initial conditions of each new subproblem $G_{p\eta}$ are set with the solution of the previous one.

After tuning the first structured controller, a destabilizing phase follows for which the system performance is degraded by introducing a $\delta^* \in \Delta$ in the system. So, the tuning method is started again adding that particular δ^* to the dynamic set Δ_a. A threshold ε is added to choose when the degradation is only marginal to exit the tuning procedure. The last phase consists in assessing the robust performance of the system over Δ_a *a posteriori*, by applying analysis tools based on outer approximations as in [30].

IV. Application to a Real Case

A. Mechanical Structure

The system under study is a medium sized expander-compressor for oil and gas applications produced by Baker Hughes Company. Fig. 5 shows a picture of the rotor under investigation and its FE modeling where the AMB at the expander side is called AMB1 and the AMB at the compressor side is called AMB2. The rotor has a mass of 236.97 kg, a length of 1.434 m, a maximum continuous speed (MCS) of 7053 rpm and a maximum speed of 7407 rpm that defines the operating frequency range of this turbomachine. The turbomachine is designed for a power rated of 2800 kW. In the delevitated state, the rotor lays on auxiliary rolling bearings that provide the minimal radial clearance of 210 μm. The rotor model was developed in the MATLAB environment following the approach described in Section II-B. Furthermore, for precise adjustment of the rotor model (3) in accordance with experimental measurements of the rotor frequency responses, the methodology outlined by Wroblewski et al. [20] was employed to refine the parameters associated with the rotor model, specifically the uncertain stiffness values. The rotor open-loop frequency responses were found

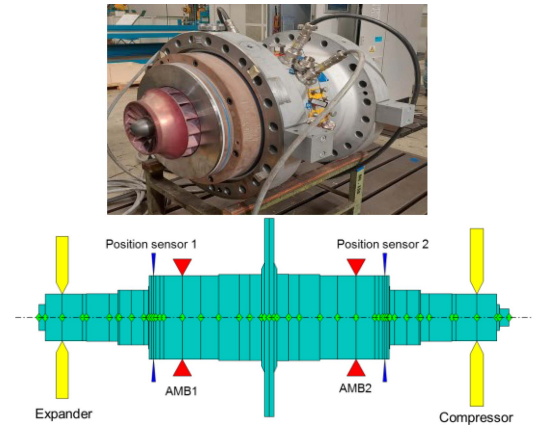

Fig. 5. Rotor picture and its FE modeling, the red triangles are the bearings, the yellow elements are the disks, and the blue elements are the sensors.

directly exploiting AMBs. Current sine sweeps were injected over the range 1–5000 Hz, during levitation obtained with a trial controller for a fixed rotational speed (from standstill to the max speed). In particular, sine sweep forces were injected by each control axis one at a time while the displacements at the position sensors were recorded. The open-loop rotor frequency responses measured at the AMBs are extracted from the closed-loop measurements according to method presented in [36]. Fig. 6 reports both the measured and modeled rotor frequency responses at standstill measured on the same control axis. For what concerns the stator part, it is found to be much stiffer than the rotor part, so the influence of its dynamics is not considered in this system.

B. Electrical Components and Controller

Regarding the electric components, the position sensors are inductive sensors, and their dynamics is modeled with a low pass filter of the first order with a band of 3 kHz. The AMBs and the amplifiers are modeled with a second order low pass filter with a cut frequency of 2.5 kHz. The two radial AMBs are equal, and they are associated with a negative stiffness of about -10^7 N/m. Finally, the controller is composed of four SISO augmented PIDs to control the two radial AMBs. The augmented PIDs present the structure described in Section II-B. Referring to (6), for this system, $D(s)$ takes into consideration the delay introduced by the sampling and the processing time related to the implementation of the augmented PIDs estimated as few tens of microseconds, and to the effect of the DAC, that is a zero-order hold with a sampling frequency, f_{DAC} of 23 kHz. Every augmented PID presents the same number of lead-lag filters, one of the first order and four of the second order whose structures are described in (7) and (8).

C. System Objectives and Constraints

In this section the requirements of (9) needed to obtain the automatic tuning of an augmented PID (with a generic number of filters) for an AMB system are derived, with particular focus on

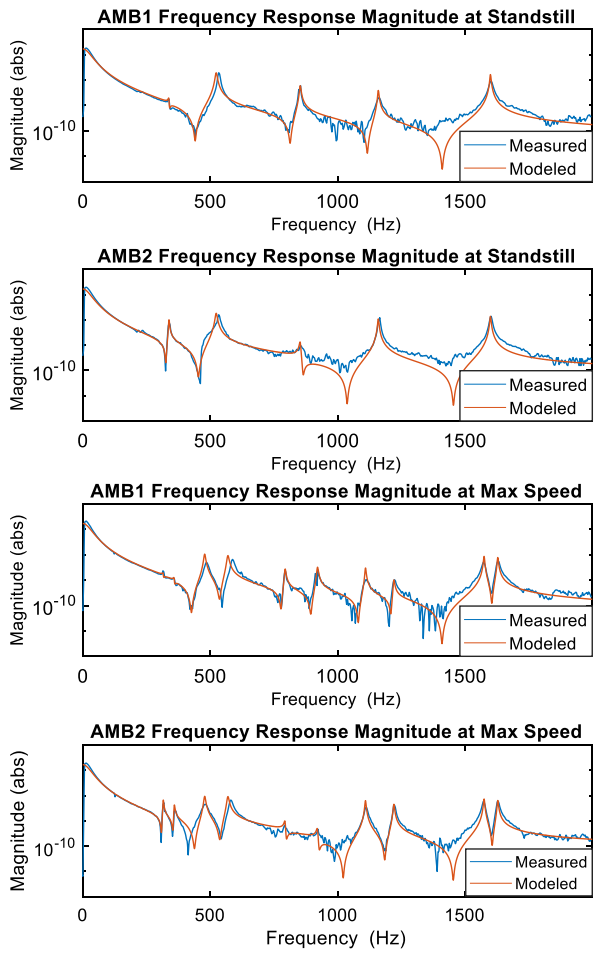

Fig. 6. Measured and modeled frequency response magnitude of the rotor at AMBs on the same control axis.

AMB oil and gas regulations. As anticipated in the previous section, imposing a *soft* requirement means to find a function that the algorithm seeks to minimize below a desired target value that can change in frequency. Conversely, if the requirement is designated as a *hard* constraint, the objective is to grant that a certain relation is respected. More precisely, referring to (10), *soft* $f_i(p,\delta)$ and *hard* $g_i(p,\delta)$ constraints are scaled each relative to the respective desired target values. These target values were chosen based on the current regulations, AMB physical limitations and empirical rules based on experience. Specifically, the regulations taken into consideration are ISO-14839 [14] API-617 [15], which concern generic AMB systems and those for oil and gas applications, respectively. Table I summarizes the *hard* and *soft* requirements imposed and their respective target values. API-617 requires that the model maximum error between the frequencies of the rotor bending modes in the operational frequency range (the first two) must be lower than 5% of their values with respect to the measurements. This condition is widely respected, as shown by Fig. 6.

1) Selection and Implementation of the Hard Constraints: As already said, the hard constraints are imposed to cope with regulation limits and feasibility. First of all, API 617 imposes the internal stability of the closed loop system. Therefore, the

TABLE I
REQUIREMENT LIST AND VALUES

Type	NAME	Purpose	Value	Frequency interval (Hz)
Hard	$g_1(p)$	Internal stability	–	$[0,\infty)$
Hard	$g_2(p)$	Sensitivity function gain	3 V/V	$[0,\infty)$
Hard	$g_3(p)$	AMB stiffness	AMB1: 2.20×10^7 N/m AMB2: 1.47×10^7 N/m	$[0{,}150\%MCS]$ $[0{,}150\%MCS]$
Soft	$f_1(p)$	Mode damping	0.30	$[0{,}150\%MCS]$
Soft	$f_2(p)$	Augmented PID gain	15 V/V 1 V/V	$[0{,}2000]$ $[2000,\infty)$
Soft	$f_3(p)$	Stability margins	25°, 2 dB	$[0{,}150\%MCS]$

Summary of imposed requirements and the respective values.

first *hard* constraint $g_1(p)$ implicitly implements it in the tuning algorithm by letting the spectral abscissa $\alpha(A)$ satisfying the following inequality:

$$\max_{\delta\in\Delta} \alpha\left(A(p,\delta)\right) < 0 \tag{13}$$

where $\alpha\ (A) = \max\{\mathrm{Re}(\varphi):\ \varphi \text{ eingevalue of } A(p,\delta)\}$ and $A(p,\delta)$ is the state matrix of the closed-loop system.

The second *hard* constraint $g_2(p)$ concerns the minimum robustness of the AMB system to noise. In fact, according to ISO-14839, the sensitivity function gain must be less than 3 for the new turbomachines equipped with AMBs. In this respect, by regulation, the sensitivity function $S(s)$ is defined as

$$S\left(s\right) = \left(I - G_p\left(s\right)G_c\left(s\right)\right)^{-1} \tag{14}$$

where for simplicity $G_p\left(s\right) = G_s\left(s\right)G_{\mathrm{rot}}(s)G_{\mathrm{act}}(s)$ is the plant transfer function and $G_{\mathrm{rot}}\left(s\right) = C_R\left(sI - A_R\right)^{-1}B_R$ describes the dynamics of the inherently unstable rotor equipped with AMBs. Hence, the function $g_2(p,\delta)$ is defined as

$$g_2\ (p,\delta) = \|W_S\left(s\right)S\left(s,p,\delta\right)\|_\infty \tag{15}$$

where $W_S(s)$ is the maximum target gain profile, that in this case is equal to 3.

The third *hard* constraint $g_3(p,\delta)$ imposes a bearing minimum stiffness. The calculation of this minimum stiffness derives from experience, and it is established on the turbomachine specific characteristics (rotor weight and length, plant power, and rotational speed) and the plant operational characteristics (process gas and plant environmental characteristics). For the considered machine, the stiffness minima are, respectively, 2.20×10^7 N/m for AMB1 and 1.47×10^7 N/m for AMB2 in the operational frequency range. To impose this constraint an upper gain limitation on the compliance function $K\ (s) = G_{\mathrm{rot}}^{-1}(s)(I - G_{\mathrm{act}}(s)G_c(s)G_s(s))$ at AMBs, the inverse of the stiffness function, was used. Hence, the third *hard* constraint is defined as

$$g_3\ (p,\delta) = \|W_{Ki}\left(s\right)K_{lm}\left(s,p,\delta\right)\|_\infty \tag{16}$$

where $i = 1,\ 2$ and $W_{K1}(s)$ and $W_{K2}(s)$ are the inverses of the minimum target stiffnesses at the two AMBs; moreover,

specifying the degrees of freedom (l, m) where AMB1 and AMB2 act, and K_{lm} indicates the stiffness function evaluated at these (l, m) freedom degrees.

2) Selection and Implementation of the Soft Constraints: *Soft* constraints are related to the optimization of the controller performance, so the main factors related to the plant design are taken into account to derive them. The API-617 limits the displacement of the rotor due to the unbalance action that is one of the greatest contributions of the external forces. Unbalance forces are synchronous with the speed of the rotor and are caused by the presence of unbalanced masses with respect to the axis of rotation of the rotor. Unbalance is due to inevitable manufacturing imperfections or to rotor wear and characterizes a particular turbomachine. For a given axis Z, at a fixed rotor speed Ω the unbalance force assumes the form

$$F_{un_z} = \Omega^2 U \cos(\Omega t + \phi) \tag{17}$$

where ϕ is the phase of the unbalance with respect to the other axis and U is the unbalance magnitude in kgm. The API 617 defines some test unbalances related to the rotor dimension, typology, and MCS, to determine the magnitude of the system displacements due to unbalance and based on the air gap of the machine. Moreover, API-617 defines the frequency range that goes from 0 rpm to 150% MCS in which the rotor vibration displacements must be limited. Moreover, in compliance with API-617 standards, the amplification factor (AF) is introduced as a measure based on the sharpness of the peak gain of a mode, aiding in the assessment of its damping characteristics. This parameter plays a crucial role in determining whether a vibration mode exhibits sufficient damping to meet the specified criteria for the system vibration performance. Specifically, API defines the AF as the ratio of the peak frequency of a mode and its -3 dB bandwidth and set its limit value to 2.5.

For this reason, the first *soft* objective $f_1(p, \delta)$ focuses on optimizing the damping of modes within the operational frequency range. In this case, the requirement function $f_1(p, \delta)$ reflects the relative satisfaction or violation of the goal. It assumes a value below 1 if the minimum damping required is satisfied and a value greater than 1 if it is not. In this respect, for the system under study, a minimum value of 0.30 for the damping ratio was set within the specified frequency range. This value is considered high enough to ensure good suppression of vibrations (low AF) and limits the magnitudes of displacements resulting from unbalance in the rotor.

The second *soft* requirement $f_2(p)$ concerns minimizing the controller gain of each augmented PID $|G_{ci}(j\omega)|$ to reduce the requested AMB coil current and to maintain the working conditions as far as possible from amplifier saturation and limit heat dissipation. The related function $f_2(p)$ is built as follows:

$$f_2\ (p) = \|W_C\,(s)\, G_{ci}\,(s, p)\,\|_\infty \tag{18}$$

where $W_C(s)$ is the maximum target gain profile chosen to grant that the amplifier saturation limit is not reached in all operating conditions. More specifically, to grant system reliability, the target gain profile is selected so that the amplifier voltage remains below 50% of the maximum voltage to meet the safety margin derived from API-617 and it is calculated by considering the system dynamic behavior based both on the API-617 unbalance tests and on the mean external forces acting on the particular turbomachine (process gas forces, stator movements) whose magnitude is derived instead from the experience in the field. Specifically, for this case study of $G_{ci}(s, p)$ is 15 V/V in the frequency range [0, 2000] Hz and 1 V/V in the frequency range [2000, ∞] Hz.

Finally, the third and last considered *soft* objective $f_3(p)$ arises from experience and regards the stability margins of the closed loop to ensure a minimum level of robust stability. Given that electrical components such as sensors, cables, amplifiers, and electromagnets may deviate from their nominal behavior, especially in the plant worksite where environmental factors can influence system behavior, gain changes and phase delays of the open-loop transfer function may occur. The function $f_3(p)$ in this case is defined as

$$f_3\ (p, \delta) = \|2\gamma D^{-1} S\,(s)\, D - \gamma I\|_\infty \tag{19}$$

where $S(s)$ is the sensitivity function defined in (14), D is an automatically computed loop scaling factor involved in computing MIMO stability margins and γ is a scalar parameter computed from the requested gain and phase margin. The closed-loop system stability margins are calculated using a disk margin of radius γ that quantify the stability against gain and phase variations in the open-loop system, as described in [37] and [38]. In a MIMO system, the disk radius γ determines the gain and the phase margins that can independently vary in each channel across all values of $\delta \in \Delta$ to ensure stability in the system closed loop. For this system under study, a phase margin of 25° and a gain margin of 2 dB were implemented in the frequency range [0, 150%MCS].

3) Uncertainty Modeling: Regarding the uncertainties, the rotational speed is considered as an uncertain real parameter δ_Ω. This allows to model the variable gyroscopic contribution linked to the rotor speed Ω, according to (2) and (3). The range of this uncertainty is selected as

$$\delta_\Omega \in [0,\ \Omega_{\max}] \tag{20}$$

where $\Omega_{\max}$ is 150% of the MCS, thus considering a safety coefficient, which grants the machine always operating within this range [39]. Moreover, even if the rotor model is updated in accordance to the experimental measurements, uncertainties on the rotor bending mode frequencies are introduced to make the system robust and cope with the model residual inaccuracies, and wear that can change the plant dynamics over time [21]. Hence, using the modal coordinates of system [40], it is possible to introduce uncertainties on the natural frequencies λ_i of the rotor bending modes as the following:

$$\delta_{\lambda i} = \lambda_i\ (1 + \delta_i)\,. \tag{21}$$

For the system under study, an uncertainty δ_i of 20 Hz was used for the first five bending modes that widely accounts for the model inaccuracies and also for possible rotor dynamics changes over time due to wear or malfunctions in the plant.

To conclude, the controller tunable parameters are constrained by physical limits, including amplifier power and electrical

TABLE II
TUNABLE PARAMETER LIMITS AND INITIALIZATION VALUES

Symbol	PARAMETER NAME	Parameter variation range	Parameter initialization
K_{Pi}	Proportional gain	[0.4 1.1]	0.65
K_{Ii}	Integral gain	60	60
τ_i	First order filter zero	[30, 200] Hz	35 Hz
α_i	First order filter pole/zero ratio	[0.2, 1]	0.85
ω_{pi}	Second order pole natural frequency	[30, 2000] Hz	150 Hz
δ_{pi}	Second order pole damping ratio	[0.05, 1]	0.70
ω_{zi}	Second order zero natural frequency	[30, 2000] Hz	150 Hz
δ_{zi}	Second order zero damping ratio	[0.05, 1]	0.70

Summary of the tunable parameter limits and initialization values used for this system under study.

system bandwidths. Table II outlines these limits and the corresponding tuning algorithm initialization values for the studied system. The initial parameters are chosen to obtain a simple controller which implements only the first order filter to partially stabilize with a positive phase [12] the first modes of the rotor, with gains sufficient to stabilize the AMB negative stiffness. The poles and zeros of the other filters are all superimposed, so their effect is null. In addition, the parameters K_{Ii} (6) are considered fixed values, as they do not directly impact on the requirements presented in this section.

V. EXPERIMENTAL RESULTS

In this section, the results are presented, with a particular emphasis on the successful attainment of all the specified and standard requirements. The tuning process was conducted in the MATLAB environment using the robust control toolbox that implements the algorithm described in Section III (systune function) and natively handles uncertain systems, on an Intel processor i7-12800H (2.40 GHz) equipped with 16 GB RAM, and it was completed within approximately 7 h. The obtained tuned controller complies with all the specified requirements described in the previous section considering all the uncertainties varying independently. Finally, to validate the controller performance, the tuned controller was tested on the real system exploiting the plant control hardware. This hardware is designed for precise calculations within specific timeframes, dependent on the particular structure of the implemented controller, and allows for the selection of the tunable parameters. The experimental results are measured exploiting the AMBs, as described in the Section III and more in detail in [36]. Fig. 7 shows the obtained controller transfer function Bode diagram for the two AMBs referring to a control axis that satisfies the *soft* controller gain requirement stated in Table I. Regarding the first *hard* constraint, through a μ analysis, the system stability was assessed for all the uncertainties, described in the previous section, showing that the stability margin is higher than 1 for all the frequencies.

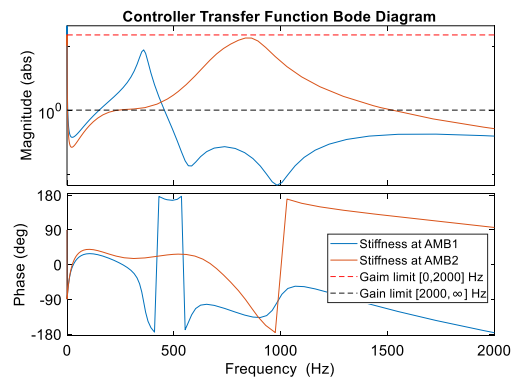

Fig. 7. Obtained AMBs controller frequency response where the dash lines refer to the controller gain limits reported in Table I.

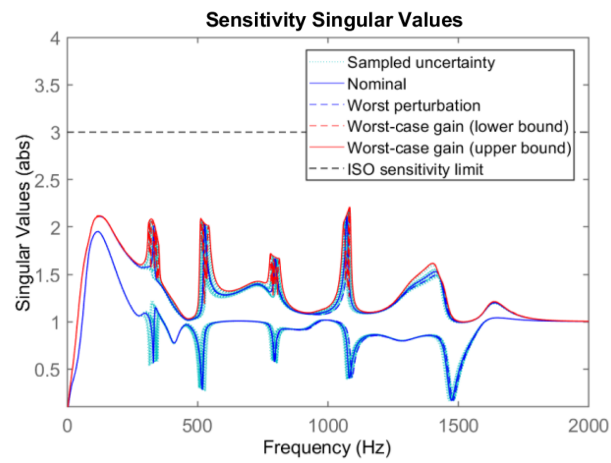

Fig. 8. Sensitivity singular values.

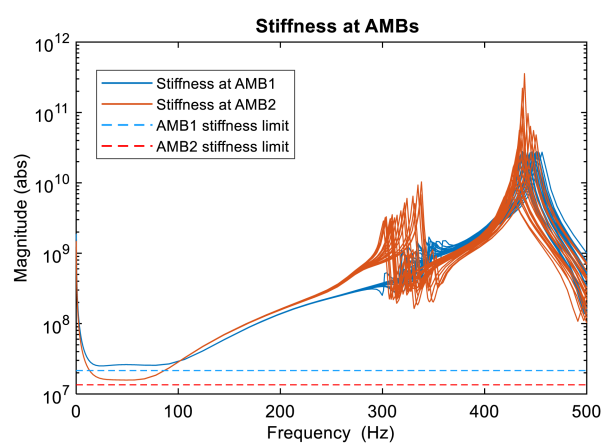

Fig. 9. Stiffnesses at bearings obtained by 1000 Monte Carlo runs, the limit values are reported in Table II.

For what concerns the *second* hard constraint regarding the sensitivity function, a singular value analysis, reported in Fig. 8, shows that the constraint is satisfied for all the frequencies and for all the uncertainties. Fig. 9 shows the stiffness at AMBs obtained by Monte Carlo simulations (1000 runs) varying the

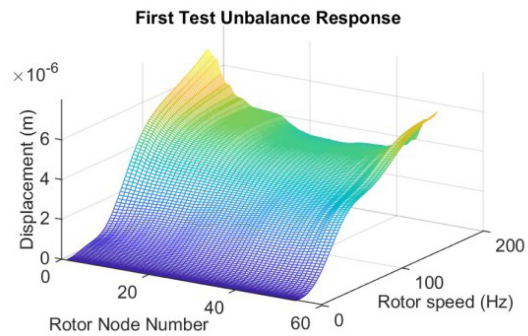

Fig. 10. First test unbalance response with the aim of exciting the first rigid mode. The maximum displacement is 7.29 μm.

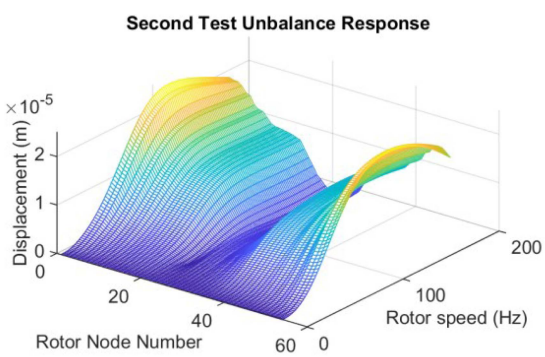

Fig. 11. Second test unbalance response with the aim of exciting the second rigid mode. The maximum displacement is 24.09 μm.

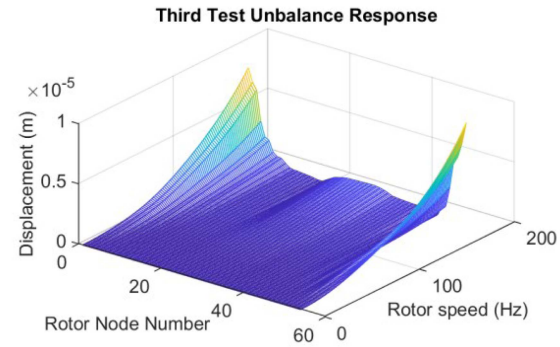

Fig. 12. Third test unbalance response with the aim of exciting the first bending mode. The maximum displacement is 8.63 μm.

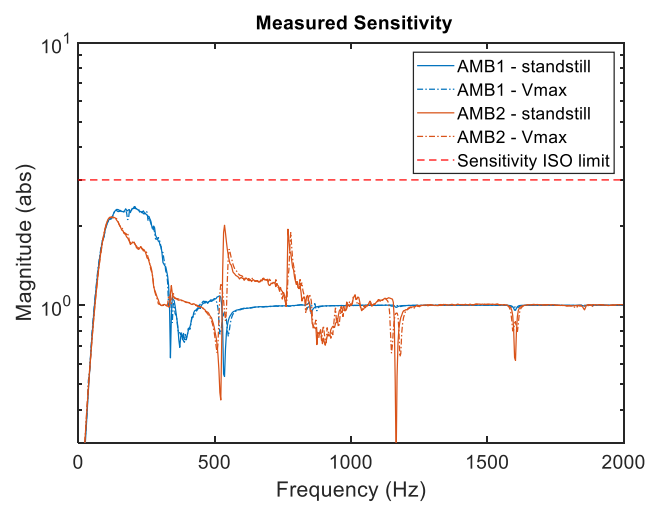

Fig. 13. Sensitivities at standstill and at maximum speed measured at AMBs.

uncertain parameters. As shown, the third *hard* constraint is satisfied for all the frequencies. To ensure that the minimum damping imposed is sufficient, the response to some test unbalances is evaluated to assess the modes AF and the compliance with the maximum vibration amplitude. For this rotor, the amplitude vibration limit is 45 μm (according to the ISO-14839) and the modes AF must be lower than 2.5 in the operating speed range (according to API-617). The used test unbalances are determined based on the mass-length excitation $U_m = 4.5 \times 10^{-4}$ kgm, with a calculation procedure specified in the API. All the three test unbalances specified by API were used to verify that the tuned controller maintains displacement and AF within the limits. Specifically, the unbalances used for testing the controller are the following. The first is an unbalance obtained positioning U_m at the center of gravity of the rotor, which excites its first rigid mode. The second is obtained by placing two $U_m/2$ unbalances at the extremities of the rotor, with opposite phases, which stimulates the second rigid mode. Finally, the third is obtained with three unbalances, $U_m/2$ one at the center of the rotor and two $U_m/4$ at the extremities with opposite phases relative to the center unbalance, which excite the first bending mode.

In order to comprehensively evaluate the system performance in the presence of diverse mode uncertainties, Figs. 10–12 present the response to test unbalances for the most critical scenarios, specifically, the ones with the lowest damping ratio of the excited modes with the added unbalances. These worst-case examples allow to assess the system robustness and response in a rigorous manner, considering the impact of the least favorable combination of uncertainties.

As shown by the figures, the maximum displacement found (in the second test unbalance) is satisfying the amplitude vibration limit (45 μm). Moreover, the AF of the modes is much lower than the API limit (2.5) in the frequency range of interest [0, 176] Hz. Regarding the imposed stability margins in Table I, they are satisfied for all the uncertainties and specified frequencies, and they are not reported in the result section only for reasons of space.

To evaluate the performance compliance of the tuned controller, rigorous testing was conducted on the real system. Figs. 13 and 14 show respectively the sensitivity measures at the AMBs and the stiffness measures at AMBs. In both the cases the measurements respect the imposed limits and are in line with the modeled outcomes, as any disparities between the model and the actual system are effectively managed through the provided control robustness. The obtained measurements showcase the effectiveness of the proposed automatic tuning technique in achieving the prescribed system performance and stability objectives. Through rigorous analysis and optimization, the controller was able to comply with both the *soft* and *hard* requirements, showcasing its adaptability and robustness for real-world scenarios.

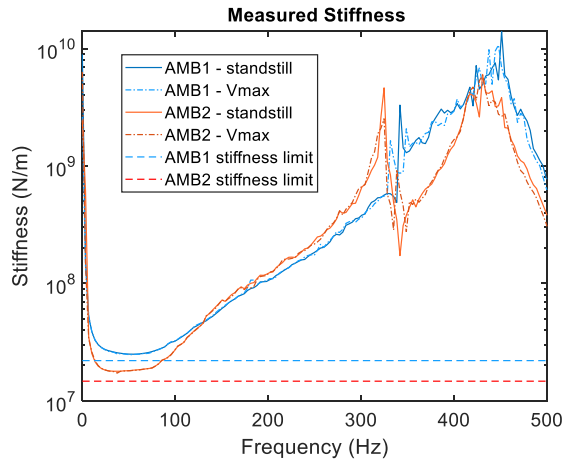

Fig. 14. Stiffnesses at standstill and at maximum speed measured at AMBs.

VI. Conclusion

In conclusion, this article introduces a novel highly adaptable and efficient augmented PID automatic tuning technique for a generic turbomachine equipped with AMBs. The method employs a nonsmooth optimization algorithm that fulfills some requirements while accounting for potential modeling errors translated into system uncertainties to enhance controller robustness. The requirements are divided into *hard* ones that serve as the fundamental constraints that the system must meet and the *soft* ones that represent the desirable characteristics that should be optimized. Through the definition of the requirements, this article offers a concise and comprehensive methodology for integrating regulation and "best practice" guidelines, with a particular attention to applications in oil and gas industry, into the tuning process enabling a fully automatic tuning of the controller parameters. The method key strengths include ease of adaptability to various AMB systems and its flexibility to accommodate different requirements. This approach is exemplified through a practical application on real-world machinery, providing a clear demonstration of its efficacy and applicability in industrial contexts. Results from the system under study demonstrate remarkable vibration suppression, appropriate dynamic response, and overall system robustness. Moreover, compared to time-consuming manual tuning methods, the proposed technique requires only around 7 h of computation for the specific case under investigation. This study offers valuable insights into advanced control techniques for magnetic bearing systems and paves the way for potential industrial adoption, leading to more efficient and stable real-world operations. Finally, the proposed approach opens the way to an automated fine-tuning of the controller parameters directly using the plant hardware.

References

[1] G. Schweitzer, "Active magnetic bearings-chances and limitations," in *Proc. 6th Int. Conf. Rotor Dyn., Int. Centre Magn. Bearings*, 2002, pp. 1–14.

[2] L. Breńkacz, L. Witanowski, M. Drosińska-Komor, and N. Szewczuk-Krypa, "Research and applications of active bearings: A state-of-the-art review," *Mech. Syst. Signal Process.*, vol. 151, Apr. 2021, Art. no. 107423, doi: 10.1016/j.ymssp.2020.107423.

[3] H. Bleuler et al., *Magnetic Bearings: Theory, Design, and Application to Rotating Machinery*. Berlin, Germany: Springer, 2009.

[4] H. Wang, Z. Wu, K. Liu, J. Wei, and H. Hu, "Modeling and control strategies of a novel axial hybrid magnetic bearing for flywheel energy storage system," *IEEE/ASME Trans. Mechatron.*, vol. 27, no. 5, pp. 3819–3829, Oct. 2022, doi: 10.1109/TMECH.2022.3145705.

[5] W. Muhao, M. O. T. Cole, and P. S. Keogh, "New LMI based gain-scheduling control for recovering contact-free operation of a magnetically levitated rotor," *Mech. Syst. Signal Process.*, vol. 96, pp. 104–124, Nov. 2017, doi: 10.1016/j.ymssp.2017.04.008.

[6] M. Hutterer and M. Schroedl, "Stabilization of active magnetic Bearing systems in the case of defective sensors," *IEEE/ASME Trans. Mechatron.*, vol. 27, no. 5, pp. 3672–3682, Oct. 2022, doi: 10.1109/TMECH.2021.3131224.

[7] M.-J. Jang, C.-L. Chen, and Y.-M. Tsao, "Sliding mode control for active magnetic bearing system with flexible rotor," *J. Franklin Inst.*, vol. 342, no. 4, pp. 401–419, Jul. 2005, doi: 10.1016/j.jfranklin.2005.01.006.

[8] A. H. Pesch, A. Smirnov, O. Pyrhönen, and J. T. Sawicki, "Magnetic bearing spindle tool tracking through μ-synthesis robust control," *IEEE/ASME Trans. Mechatron.*, vol. 20, no. 3, pp. 1448–1457, Jun. 2015, doi: 10.1109/TMECH.2014.2344592.

[9] D. Benjamin, T. Alban, and J. Mahfoud, "Assessment of the effectiveness of a polar fuzzy approach for the control of centrifugal compressors," *J. Dynamic Syst., Meas., Control, ASME*, vol. 136, no. 4, 2014, Art. no. 041004, doi: 10.1115/1.4026468.

[10] J. Laldingliana and P. K. Biswas, "Artificial intelligence based fractional order PID control strategy for active magnetic bearing," *J. Elect. Eng. Technol.*, vol. 17, pp. 3389–3398, 2022, doi: 10.1007/s42835-022-01102-6.

[11] C. Gähler, "Rotor dynamic testing and control with active magnetic bearings," Ph.D. dissertation, ETH, Zurich, 1998, doi: 10.3929/ethz-a-001987464.

[12] B. Defoy, "Investigation on the control of supercritical centrifugal compressors supported by active magnetic bearings: Toward a new control strategy?," Ph.D. dissertation, INSA de Lyon, Lyon, 2012.

[13] J. Schmied and A. Kosenkov, "Practical controller design for rotors on magnetic bearings by means of an efficient simulation tool," in *Turbo Expo: Power for Land, Sea, and Air*, vol. 55270, p. V07BT30A021, San Antonio, TX, USA, Jun. 2013.

[14] *Mechanical Vibration—Vibration of Rotating Machinery Equipped With Active Magnetic Bearings*, ISO 14839-3, 2006.

[15] API Standard 617, *Axial and Centrifugal Compressors and Expander Compressors for Petroleum, Chemical and Gas Industry Services*, 8th ed., Washington, DC, USA: American Petroleum Institute, 2014.

[16] P. Apkarian, "Tuning controllers against multiple design requirements," in *Proc. 16th Int. Conf. System Theory, Control Comput.*, 2012, pp. 1–6.

[17] P. Apkarian, P. Gahinet, and C. Buhr, "Multi-model, multi-objective tuning of fixed-structure controllers," in *Proc. Eur. Control Conf.*, 2014, pp. 856–861, doi: 10.1109/ECC.2014.6862200.

[18] P. Apkarian, M. N. Dao, and D. Noll, "Parametric robust structured control design," *IEEE Trans. Autom. Control*, vol. 60, no. 7, pp. 1857–1869, Jul. 2015, doi: 10.1109/TAC.2015.2396644.

[19] A. Noshadi, J. Shi, W. S. Lee, P. Shi, and A. Kalam, "System identification and robust control of multi-input multi-output active magnetic bearing systems," *IEEE Trans. Control Syst. Technol.*, vol. 24, no. 4, pp. 1227–1239, Jul. 2016, doi: 10.1109/TCST.2015.2480009.

[20] A. C. Wroblewski, J. T. Sawicki, and A. H. Pesch, "Rotor model updating and validation for an active magnetic bearing based high-speed machining spindle," *J. Eng. Gas Turbines Power*, vol. 134, no. 12, 2022, Art. no. 122509.

[21] G. Donati, M. Basso, G. A. Manduzio, M. Mugnaini, T. Pecorella, and C. Camerota, "A convolutional neural network for electrical fault recognition in active magnetic bearing systems," *Sensors*, vol. 23, no. 16, 7023, Art. no. 2023.

[22] C. Wei and D. Söffker, "Optimization strategy for PID-controller design of AMB rotor systems," *IEEE Trans. Control Syst. Technol.*, vol. 24, no. 3, pp. 788–803, May 2016, doi: 10.1109/TCST.2015.2476780.

[23] E. E. Swanson, E. H. Maslen, G. Li, and C. H. Cloud, "Rotordynamic design audits of AMB supported machinery," in *Proc. 37th Turbomachinery Symp.*, 2008, pp. 133–158.

[24] M. Lalanne and G. Ferraris, *Rotordynamics Prediction in Engineering*. Hoboken, NJ, USA: Wiley, 1998.

[25] M. I. Friswell, J. E. Penny, S. D. Garvey, and A. W. Lees, *Dynamics of Rotating Machines*. Cambridge, MA, USA: Cambridge Univ. Press, 2010.

[26] P. Apkarian, "Internet pages," 2010. [Online]. Available: http://pierre.apkarian.free.fr

[27] K. Zhou, J. C. Doyle, and K. Glover, *Robust and Optimal Control*. Englewood Cliffs, NJ, USA: Prentice Hall, 1996.
[28] S. Skogestad and I. Postlethwaite, *Multivariable Feedback Design - Analysis and Design*. Hoboken, NJ, USA: Wiley, 1996.
[29] J. D. Blight, R. L. Dailey, and D. Gangsaas, "Practical control law design for aircraft using multivariable techniques," *Int. J. Control*, vol. 59, no. 1, pp. 93–137, 1994.
[30] M. K. H. Fan, A. L. Tits, and J. C. Doyle, "Robustness in the presence of mixed parametric uncertainty and unmodeled dynamics," *IEEE Trans. Autom. Control*, vol. 36, no. 1, pp. 25–38, Jan. 1991.
[31] P. Gahinet and P. Apkarian, "Decentralized and fixed-structure H_∞ control in MATLAB," in *Proc. 50th IEEE Conf. Decis. Control Eur. Control Conf.*, 2011, pp. 8205–8210, doi: 10.1109/CDC.2011.6160298.
[32] J. Doyle, K. Glover, P. Khargonekar, and B. Francis, "State-space solutions to standard H_2 and H_∞ control problems." in *Proc. Amer. Control Conf.*, Atlanta, GA, USA, 1988, pp. 1691–1996, doi: 10.23919/ACC.1988.4789992.
[33] R. Fletcher, *Practical Methods of Optimization*. Hoboken, NJ, USA: Wiley, 1987.
[34] F. H. Clarke, *Optimization and Nonsmooth Analysis*, ser. Canadian Math. Soc. Series. New York, NY, USA: Wiley, 1983.
[35] P. Apkarian and D. Noll, "Nonsmooth H∞ synthesis," *IEEE Trans. Autom. Control*, vol. 51, no. 1, pp. 71–86, Jan. 2006, doi: 10.1109/TAC.2005.860290.
[36] J. T. Sawicki and E. T. Maslen, "Accurate identification of plant model for robust control of an AMB machine tool spindle," in *Proc. 9th Int. Conf. Motion Vib. Control*, 2008.
[37] J. D. Blight, R. L. Dailey, and D. Gangsaas, "Practical control law design for aircraft using multivariable techniques," *Int. J. Control*, vol. 59, no. 1, pp. 93–137, Jan. 1994, doi: 10.1080/00207179408923071.
[38] P. Seiler, A. Packard, and P. Gahinet, "An introduction to disk margins [Lecture Notes]," *IEEE Control Syst. Mag.*, vol. 40, no. 5, pp. 78–95, Oct. 2020, doi: 10.1109/MCS.2020.3005277.
[39] S. T. Yoon, Z. Lin, and P. E. Allaire, *Control of Surge in Centrifugal Compressors By Active Magnetic Bearings: Theory and Implementation*. Berlin, Germany: Springer, 2012.
[40] M. I. Friswell, "Candidate reduced order models for structural parameter estimation," *ASME J. Vib. Acoust.*, vol. 112, pp. 93–97, 1990.

Giovanni Donati received the B.S. and M.S. degrees in mechanical engineering from the University of Florence, Florence, Italy, in 2018 and 2021, respectively. He is currently working toward the Ph.D. degree in smart industry with the University of Pisa, Pisa, Italy.

His research interests include advanced control and fault diagnosis of magnetic bearings in high-speed rotating machinery and visual servoing of robotic systems.

Michele Basso received the master's degree in electronic engineering from the University of Florence, Florence, Italy, in 1992, and the Ph.D. degree in systems engineering from the University of Bologna, Bologna, Italy, in 1997.

From 1998 to 2010, he was an Assistant Professor with the Dipartimento di Sistemi e Informatica, University of Florence, where he is currently an Associate Professor with the Department of Information Engineering. His research interests include nonlinear dynamical systems, robust control, sensor fusion, and unmanned aerial vehicles.

Marco Mugnaini (Senior Member, IEEE) received the Laurea degree in electronic engineering and the Ph.D. degree in reliability, availability, and logistics from the University of Florence, Florence, Italy, in 1999 and 2003, respectively.

Since 2003, he has been a Product Safety Engineer with General Electric Oil and Gas business, Florence, Italy. Since 2019, he has been an Associate Professor of electronic measurements with the Department of Information Engineering, University of Siena, Siena, Italy. His research interests include the development of measurement systems based on chemical sensors.

Dr. Mugnaini was a recipient of the Green Belt Certification from General Electric Oil and Gas.

Massimiliano Ortiz Neri received the graduation degree in automation engineering from the University of Pisa, Pisa, Italy, in 1999.

After several years of work in the telecommunication industry, he joined Baker Hughes in 2005 as Control Systems Engineer working on steam turbine and electric motor driven compressors. In 2012, he moved to Compressor and Expander New Product Development Department, focusing on active magnetic bearing systems. As a Senior Principal Engineer he is currently leading activities relevant to energy transition involving turboexpander applications.